

# Fock-space relativistic coupled-cluster calculations of clock transition properties in $\text{Pb}^{2+}$

Palki Gakkhar,<sup>1</sup> Ravi Kumar,<sup>2</sup> D. Angom,<sup>3</sup> and B. K. Mani<sup>1,\*</sup>

<sup>1</sup>*Department of Physics, Indian Institute of Technology, Hauz Khas, New Delhi 110016, India*

<sup>2</sup>*Department of Chemistry, University of Zurich, Switzerland*

<sup>3</sup>*Department of Physics, Manipur University, Canchipur 795003, Manipur, India*

We have implemented an all-particle multireference Fock-space relativistic coupled-cluster theory to probe  $6s^2\ ^1S_0 - 6s6p\ ^3P_0^o$  clock transition in an even isotope of  $\text{Pb}^{2+}$ . We have computed, excitation energy for several low lying states, E1 and M1 transition amplitudes, and the lifetime of the clock state. Moreover, we have also calculated the ground state dipole polarizability using perturbed relativistic coupled-cluster theory. To improve the accuracy of results, we incorporated the corrections from the relativistic and QED effects in all our calculations. The contributions from triple excitations are accounted perturbatively. Our computed excitation energies are in excellent agreement with the experimental values for all the states. Our result for lifetime,  $9.76 \times 10^6$  s, of clock state is  $\approx 8.5\%$  larger than the previous value using CI+MBPT [Phys. Rev. Lett. **127**, 013201 (2021)]. Based on our analysis, we find that the contributions from the *valence-valence* correlations arising from higher energy configurations and the corrections from the perturbative triples and QED effects are essential to get accurate clock transition properties in  $\text{Pb}^{2+}$ . Our computed value of dipole polarizability is in good agreement with the available theoretical and experimental data.

## I. INTRODUCTION

Optical atomic clocks are one of the most accurate time measurement instruments in existence today [1, 2]. Due to their unprecedented accuracies as frequency and time standards, they can serve as important probes of fundamental phenomena in physics and function as key components in technological applications. Some examples where atomic clocks are of vital importance include, measuring the variation in the fundamental constants [3–5], probing physics beyond the standard model of particle physics [6, 7], navigation systems [8, 9], quantum computer [10, 11], the basis for redefining the second [5, 12], and others [1, 2]. For the single ion optical clocks, the hyperfine induced  $3s^2\ ^1S_0 - 3s3p\ ^3P_0^o$  (267.4 nm) transition based  $^{27}\text{Al}^+$  is demonstrated to be one of the best clocks, with a fractional frequency uncertainty of  $9.4 \times 10^{-19}$  [13]. The high accuracy in  $^{27}\text{Al}^+$  could be attributed to the low sensitivity to electromagnetic fields, narrow natural linewidth and small room temperature black-body radiation (BBR) shift in the clock transition frequency [14–16]. Among the neutral atoms, a lattice clock based on degenerate fermionic  $^{87}\text{Sr}$  atoms with a hyperfine-induced  $5s^2\ ^1S_0 - 5s5p\ ^3P_0^o$  (698 nm) transition is reported to be one of the best neutral atom clocks. The smallest fractional frequency error achieved is  $\approx 2.0 \times 10^{-18}$  [17, 18].

In the quest for a new and improved frequency standard, an optical clock based on  $6s^2\ ^1S_0 - 6s6p\ ^3P_0^o$  transition, mediated through a *two* photon E1+M1 channel, in doubly ionized even isotope of Lead ( $\text{Pb}^{2+}$ ) could be a promising candidate. Like in  $^{27}\text{Al}^+$ , the clock transition is an electric dipole forbidden transition between two  $J = 0$  states, providing a strong resistance to the environmental perturbations. In addition, unlike  $^{27}\text{Al}^+$ , the nuclear spin quantum number  $I$  is zero. This is crucial, as it prevents clock transition from the nonscalar perturbations which may arise through the coupling between the

electron and nuclear multipole moments. Despite this important prospect with  $\text{Pb}^{2+}$  as an accurate optical atomic clock, the properties of the relevant transition have not been explored in detail. For example, in terms of theoretical calculations, to the best of our knowledge, there is only one study on the lifetime of the clock state [19]. The work [19], employing a combined method of configuration interaction (CI) and many-body perturbation theory (MBPT), computed the lifetime,  $\tau$ , of the clock state,  $^3P_0^o$ , as  $9.0 \times 10^6$  s. Considering that there are no experimental data, additional theoretical calculations, specially using the accurate methods like relativistic coupled-cluster (RCC), would be crucial to get better and accurate insights on the clock properties. Moreover, the inclusion of relativistic and QED corrections to the properties calculations are essential to obtain reliable results. It can thus be concluded that there is a clear research gap in terms of the scarcity of accurate properties results for  $^1S_0 - ^3P_0^o$  clock transition of  $\text{Pb}^{2+}$ .

In this work, we have implemented an all-particle multireference Fock-space relativistic coupled-cluster (FSRCC) theory to compute the clock transition properties of  $\text{Pb}^{2+}$  accurately. It is to be noted that, RCC theory is one of the most reliable quantum many-body theories for atomic structure calculations. It accounts for electron correlation effects to all-orders of residual Coulomb interaction and has been employed to obtain accurate results in several closed-shell and one-valence atoms and ions [20–23]. The application of RCC for two-valence atomic systems, as the present case of  $\text{Pb}^{2+}$  clock transition is, however, limited to few studies [24–26]. And, the reason for this, perhaps, is the complications associated with the implementation of FSRCC theory for multi-reference systems [16, 24–26]. To address the clock transition properties in a comprehensive way, using FSRCC theory [16, 26], we carried out precise calculations of the excitation energies and E1 and M1 transition amplitudes associated with  $^1S_0 - ^3P_0^o$  transition in  $\text{Pb}^{2+}$ . Using these results, we have then calculated the lifetime of the  $^3P_0^o$  clock state. In addition, as electric dipole polarizability is a crucial parameter for estimating BBR shift in clock frequency, we have also calculated

\* bkmami@physics.iitd.ac.in

the ground state polarizability of  $\text{Pb}^{2+}$  using perturbed relativistic coupled-cluster (PRCC) theory [23, 27]. Moreover, in all these properties calculations, we have incorporated and analyzed the contributions from the Breit interaction, QED corrections and perturbative triples.

The remainder of the paper is organized into five sections. In Sec. II, we provide a brief description of the FSRCC theory for two-valence atomic systems. We have given the coupled-cluster working equation for two-valence systems. In the Sec. III, we provide and discuss the expression for E1M1 decay rate. The results obtained from our calculations are presented and analyzed in Sec. IV. Theoretical uncertainty in our computed results is discussed in Sec. V of the paper. Unless stated otherwise, all results and equations presented in this paper are in atomic units ( $\hbar = m_e = e = 1/4\pi\epsilon_0 = 1$ ).

## II. TWO-VALENCE FSRCC THEORY

Since the clock transition in  $\text{Pb}^{2+}$  involves atomic state functions (ASFs) of two-valence nature, we need an accurate multireference theory to calculate these wavefunctions and corresponding many-body energies. In the present work we have employed a FSRCC theory for two-valence [16, 26] to obtain the many-body wavefunction and corresponding energy. In Refs. [16, 26, 28], we have discussed in detail the implementation of FSRCC theory to sophisticated parallel codes and have also given the working equations and Goldstone diagrams contributing to the theory. So, here, for completeness, we provide a very brief description of FSRCC theory for two-valence atoms and properties calculations using it in the context of  $\text{Pb}^{2+}$ .

The atomic state function for a two-valence atom or ion is obtained by solving the many-body Schrodinger equation

$$H^{\text{DCB}}|\Psi_{vw}\rangle = E_{vw}|\Psi_{vw}\rangle, \quad (1)$$

where  $|\Psi_{vw}\rangle$  is the exact many-body wavefunction and  $E_{vw}$  is the corresponding exact energy. The indices  $v, w, \dots$  represent the valence orbitals.  $H^{\text{DCB}}$  is the Dirac-Coulomb-Breit no-virtual-pair Hamiltonian used in all calculations, and expressed as

$$H^{\text{DCB}} = \sum_{i=1}^N [c\alpha_i \cdot \mathbf{p}_i + (\beta_i - 1)c^2 - V_N(r_i)] + \sum_{i<j} \left[ \frac{1}{r_{ij}} + g^{\text{B}}(r_{ij}) \right], \quad (2)$$

where  $\alpha$  and  $\beta$  are the Dirac matrices, and  $1/r_{ij}$  and  $g^{\text{B}}(r_{ij})$  are the Coulomb and Breit interactions, respectively. In FSRCC theory,  $|\Psi_{vw}\rangle$  is written as

$$|\Psi_{vw}\rangle = e^T \left[ 1 + S_1 + S_2 + \frac{1}{2} (S_1^2 + S_2^2) + R_2 \right] |\Phi_{vw}\rangle, \quad (3)$$

where  $|\Phi_{vw}\rangle = a_w^\dagger a_v^\dagger |\Phi_0\rangle$ , is the Dirac-Fock reference state for a two-valence system. Operators  $T$ ,  $S$  and  $R$  are the electron excitation operators, referred to as the coupled-cluster

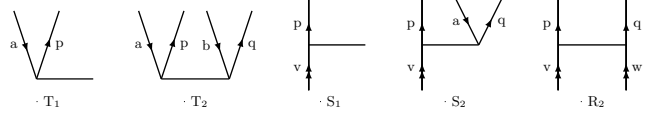


FIG. 1. The diagrammatic representation of closed-shell, one-valence, and two-valence single and double CC operators.

(CC) operators, for closed-shell, one-valence and two-valence sectors, respectively. The subscripts 1 and 2 with these operators represent the single and double excitations, referred to as the coupled-cluster with singles and doubles (CCSD) approximation. The FSRCC theory with CCSD approximation subsumes most of the electron correlation effects in atomic structure calculations and provides an accurate description of the calculated properties. In the second quantized representation, the CC operators are expressed as

$$T_1 = \sum_{ap} t_{ap}^\dagger a_a \quad \text{and} \quad T_2 = \frac{1}{2!} \sum_{abpq} t_{ab}^{pq} a_p^\dagger a_q^\dagger a_b a_a, \quad (4a)$$

$$S_1 = \sum_p s_p^\dagger a_p a_v \quad \text{and} \quad S_2 = \sum_{apq} s_{va}^{pq} a_p^\dagger a_q^\dagger a_a a_v, \quad (4b)$$

$$R_2 = \sum_{pq} r_{vw}^{pq} a_p^\dagger a_q^\dagger a_w a_v. \quad (4c)$$

Here, the indices  $a, b, \dots$  and  $p, q, \dots$  represent the core and virtual orbitals, respectively. And,  $t, s$  and  $r$  are the cluster amplitudes corresponding to  $T$ ,  $S$  and  $R$  coupled-cluster operators, respectively. The diagrammatic representation of these operators is shown in Fig. 1. It is to be however mentioned that, the dominant contributions from triple excitations are also included using perturbative triples approach [16].

The operators for closed-shell and one-valence sectors are obtained by solving the set of coupled nonlinear equations discussed in Refs. [21] and [29], respectively. The two-valence CC operator,  $R_2$ , is obtained by solving the CC equation [16, 26]

$$\langle \Phi_{vw}^{pq} | \bar{H}_N + \{ \bar{H}_N S' \} + \{ \bar{H}_N R_2 \} | \Phi_{vw} \rangle = E_{vw}^{\text{att}} \langle \Phi_{vw}^{pq} | [S' + R_2] | \Phi_{vw} \rangle. \quad (5)$$

Here, for compact notation we have used  $S' = S_1 + S_2 + \frac{1}{2} (S_1^2 + S_2^2)$ .  $E_{vw}^{\text{att}}$  is the two-electron attachment energy and it is expressed as the difference between the correlated energy of  $(n-2)$ -electron (closed-shell) and  $n$ -electron (two-valence) sectors,  $E_{vw} - E_0$ .

In Fig. 2, we have given the Goldstone diagrams contributing to *linearized* FSRCC theory for two-valence systems. These are obtained by considering the terms with only *one* order of CC operators in Eq. (5) and then contracting residual Coulomb interaction with these CC operators using Wick's theorem. The CC diagrams (l) – (n) are referred to as the folded diagrams and they arise due to renormalization

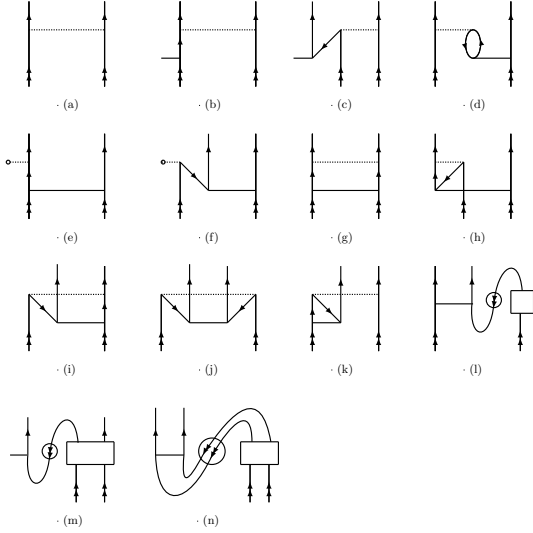


FIG. 2. The CC diagrams contributing to the *linearized* FSRCC theory for two-valence atomic systems. Diagrams (l) – (n) are referred to as the folded diagrams and arise from the renormalization terms in CC equations for multireference systems.

terms on the right hand side of Eq. (5). The presence of folded diagrams in open-shell systems constitute one of the main differences from the CC theory of closed-shell systems. The rectangular portion represents the effective energy diagrams arising from the one-valence (diagram (l)) and two-valence (diagrams (m) and (n)) sectors. The Goldstone diagrams in Fig. 2 correspond to the algebraic expression

$$\begin{aligned}
 & \langle H_N \rangle_{vw}^{pq} + \langle H_N T \rangle_{vw}^{pq} + \langle H_N S' \rangle_{vw}^{pq} + \langle H_N R_2 \rangle_{vw}^{pq} - \\
 & \langle E_{vw}^{\text{att}} S' \rangle_{vw}^{pq} - \langle E_{vw}^{\text{att}} R_2 \rangle_{vw}^{pq} = g_{pqvw} + g_{pqrw} s_v^r - \\
 & - g_{aqvw} t_a^p + \tilde{g}_{pavw} s_{av}^{rq} + g_{pqvw} \epsilon_p + g_{pqrw} r_{vw}^{rs} - \\
 & - g_{aqvr} s_{av}^{pr} + g_{abvw} t_{ab}^{pq} - g_{aqrw} s_{va}^{rp} - E_w^{\text{att}} r_{vw}^{pq} - \\
 & - E_{vw}^{\text{att}} s_v^p - E_{vw}^{\text{att}} r_{vw}^{pq}, \quad (6)
 \end{aligned}$$

where  $\tilde{g}_{ijkl} = g_{ijkl} - g_{ijlk}$ . Since we have used Dirac-Fock orbitals in our calculations, diagram (f) does not contribute, and therefore not included in the expression.

### III. E1M1 DECAY RATE USING FSRCC

Since  $I = J = F = 0$  for  $^1S_0 - ^3P_0^o$  clock transition in  $\text{Pb}^{2+}$ , it is allowed through a *two-photon* E1+M1 channel. As shown in the schematic diagram, Fig. 3, in the first route, the initial state  $|\Psi_i\rangle$  can couple to a same parity state through a magnetic dipole operator (photon with energy  $\omega_1$ ) and then connect to the final state  $|\Psi_f\rangle$  through an electric dipole operator (photon with energy  $\omega_2$ ). Alternatively, in the second route, the initial state  $|\Psi_i\rangle$  can couple to an opposite parity state via an electric dipole operator first and then connect to the ground state through a magnetic dipole operator. Mathematically, the E1+M1 decay rate from  $|\Psi_f\rangle$  to  $|\Psi_i\rangle$  can be expressed in terms of the reduced matrix elements of electric

and magnetic dipole operators, as [30, 31]

$$\begin{aligned}
 \Gamma_{E1M1} = & \frac{8}{27\pi} \alpha^6 \int_0^\infty d\omega_1 \omega_1^3 \int_0^\infty d\omega_2 \omega_2^3 \\
 & \times \left| \frac{\langle \Psi_f || \mathbf{D} || \Psi_n \rangle \langle \Psi_n || M_1 || \Psi_i \rangle}{E_n + \omega_1 - E_i} \right. \\
 & \left. + \frac{\langle \Psi_f || M_1 || \bar{\Psi}_n \rangle \langle \bar{\Psi}_n || \mathbf{D} || \Psi_i \rangle}{E_{\bar{n}} + \omega_2 - E_i} \right|^2 \\
 & \times \delta(E_i + \omega_1 + \omega_2 - E_f). \quad (7)
 \end{aligned}$$

Here for  $\text{Pb}^{2+}$ :  $|\Psi_i\rangle = 6s6p \ ^3P_0^o$ ,  $|\Psi_f\rangle = 6s^2 \ ^1S_0$ ,  $|\Psi_n\rangle = 6s6p \ ^3P_1^o$ ,  $6s6p \ ^1P_1^o$  and  $|\bar{\Psi}_n\rangle = 6s7s \ ^3S_1$ ,  $6s6d \ ^3D_1$ . Since the transition is allowed through two photons, the energy difference of final and initial states satisfies the relation  $E_f - E_i = \omega_1 + \omega_2$ .

The reduced matrix elements in Eq. (7) are calculated using the FSRCC theory. Properties calculation using FSRCC theory is explained in detail in our work [16]. However, to illustrate it briefly in the present work, we consider the example of dipole matrix element. Using the RCC wave function from Eq. (3), the dipole matrix elements is

$$\begin{aligned}
 \langle \Psi_f || \mathbf{D} || \Psi_n \rangle = & \sum_{kl} c_k^{f*} c_l^n \left[ \langle \Phi_k || \tilde{\mathbf{D}} + \tilde{\mathbf{D}} (S' \right. \\
 & + R_2) + (S' + R_2)^\dagger \tilde{\mathbf{D}} + (S' + R_2)^\dagger \\
 & \left. \tilde{\mathbf{D}} (S' + R_2) || \Phi_l \rangle \right], \quad (8)
 \end{aligned}$$

where the coefficients  $c_k^f$  represent the mixing coefficients in the expansion of a multireference configuration state function  $|\Phi_f\rangle$ . These are obtained by diagonalizing the  $H^{\text{DCB}}$  matrix within the chosen model space. The dressed operator  $\tilde{\mathbf{D}} = e^{T^\dagger} \mathbf{D} e^T$ , is a non terminating series in closed-shell CC operator  $T$ . Including all orders of  $T$  in the dressed operator is practically challenging. In Ref. [29], we developed an algorithm to include a class of dominant diagrams to all order in  $T$ , iteratively, in the dressed Hamiltonian. Based on this study, we concluded that the terms higher than quadratic in  $T$  contribute less than 0.1% to the properties. So, in the present work, we truncate  $\tilde{\mathbf{D}}$  after the second-order in  $T$  and include  $\tilde{\mathbf{D}} \approx \mathbf{D} + \mathbf{D}T + T^\dagger \mathbf{D} + T^\dagger \mathbf{D}T$  terms in the properties calculation.

### IV. RESULTS AND DISCUSSIONS

#### A. Single-particle basis and convergence of properties

An accurate description of single-electron wave functions and corresponding energies are crucial to obtain the reliable results using FSRCC theory. In the present work, we have used the Gaussian-type orbitals (GTOs) [32] as the single-electron basis for FSRCC calculations. The GTOs are used as the finite basis sets in which the single-electron wave functions are expressed as a linear combination of the Gaussian-type functions (GTFs). More precisely, the GTFs of the large

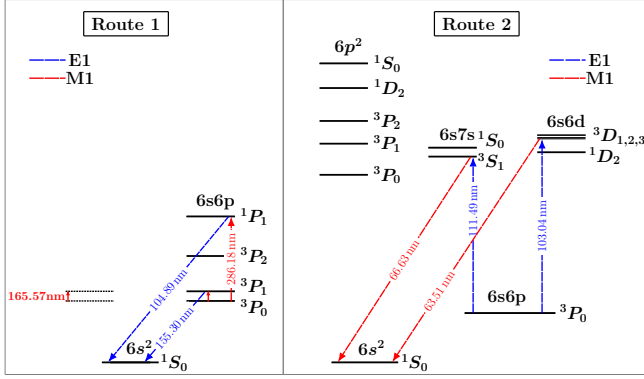


FIG. 3. Schematic energy level diagram for  $6s^2 \ ^1S_0 \rightarrow 6s6p \ ^3P_0^o$  clock transition in  $\text{Pb}^{2+}$  via a two-photon E1+M1 transition.

component of the wavefunction are expressed as

$$g_{\kappa p}^L(r) = C_{\kappa i}^L r^{n_{\kappa}} e^{-\alpha_p r^2}, \quad (9)$$

where  $p = 0, 1, 2, \dots, N$  is the GTO index and  $N$  is the total number of GTFs. The exponent  $\alpha_p$  is further expressed as  $\alpha_0 \beta^{p-1}$ , where  $\alpha_0$  and  $\beta$  are the two independent parameters. The parameters  $\alpha_0$  and  $\beta$  are optimized separately for each orbital symmetry so that the single-electron wavefunctions and energies match well with the numerical values obtained from the GRASP2K [33]. The small components of wavefunctions are derived from the large components using the kinetic balance condition [34].

In Table I, we have provided the optimized values of  $\alpha_0$  and  $\beta$  parameters for  $\text{Pb}^{2+}$  and have compared the values of single-electron and self-consistent field (SCF) energies with GRASP2K [33] and B-spline [35] results. It is to be mentioned that, the single-electron basis used in the properties calculations also incorporates the effects of Breit interaction, vacuum polarization and the self-energy corrections. As evident from the table, the single-particle and SCF energies are in excellent agreement with GRASP2K and B-spline results. The largest difference at the level of SCF and single-particle energies are 0.0001% and 0.0003%, respectively.

Since GTOs are a mathematically incomplete basis, convergence of the properties results with basis size must be checked to get reliable results using FSRCC. To show the convergence of properties results, in Table VIII of Appendix, we have listed the values of electric dipole polarizability and E1 and M1 transition reduced matrix elements with increasing basis size. To obtain a converged basis, we start with a moderate basis size and add orbitals systematically to each symmetry until the change in the properties is less than or equal to  $10^{-3}$  in respective units. For example, as evident from the table, the change in E1 amplitude of  $\langle ^1S_0 || D || ^1P_1^o \rangle$  transition is of the order of  $10^{-3}$  a.u. when basis is augmented from 158 ( $24s21p18d13f8g7h$ ) to 169 ( $25s22p19d14f9g8h$ ) orbitals. So, to minimize the computation time, we consider the basis set with 169 orbitals as optimal, and use it for further FSRCC calculations where the corrections from the Breit interaction, vacuum polarization and the self-energy are incorporated.

TABLE I. The single-particle and SCF energies (in a.u.) from GTO compared with GRASP2K and B-Spline results. The optimized  $\alpha_0$  and  $\beta$  parameter for the even tempered basis used in our calculations are also provided.

Orbitals	GTO	GRASP2K	B-Spline
$1s_{1/2}$	-3257.41150	-3257.40298	-3257.41571
$2s_{1/2}$	-589.39795	-589.39605	-589.39835
$2p_{1/2}$	-565.00395	-565.00364	-565.00295
$2p_{3/2}$	-484.41530	-484.41512	-484.41548
$3s_{1/2}$	-145.26466	-145.26400	-145.26472
$3p_{1/2}$	-134.31668	-134.31639	-134.31638
$3p_{3/2}$	-116.10663	-116.10639	-116.10665
$3d_{3/2}$	-98.32473	-98.32446	-98.32473
$3d_{5/2}$	-94.48445	-94.48420	-94.48445
$4s_{1/2}$	-35.49304	-35.49280	-35.49305
$4p_{1/2}$	-30.72284	-30.72269	-30.72276
$4p_{3/2}$	-26.20738	-26.20725	-26.20737
$4d_{3/2}$	-18.43141	-18.43130	-18.43141
$4d_{5/2}$	-17.57859	-17.57861	-17.57859
$4f_{5/2}$	-7.44501	-7.44494	-7.44502
$4f_{7/2}$	-7.25330	-7.25331	-7.25331
$5s_{1/2}$	-7.63856	-7.63855	-7.63857
$5p_{1/2}$	-5.94459	-5.94458	-5.94458
$5p_{3/2}$	-5.09665	-5.09664	-5.09666
$5d_{3/2}$	-2.62373	-2.62373	-2.62373
$5d_{5/2}$	-2.51852	-2.51852	-2.51852
$E_{\text{SCF}}$	-20910.40152	-20910.37469	-20910.40151
<hr/>			
	$\alpha_0$	$\beta$	GTOs
$s$	0.00450	1.805	40
$p$	0.00478	1.792	38
$d$	0.00605	1.855	34
$f$	0.00355	1.845	28

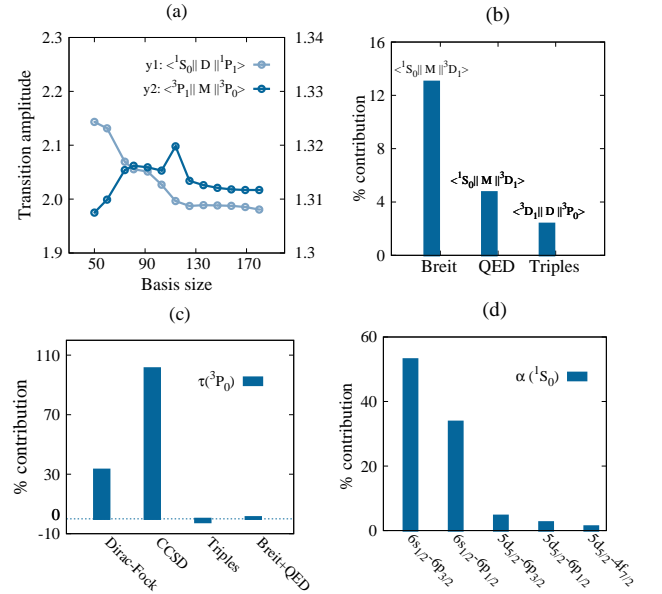


FIG. 4. Convergence of transition amplitudes with basis size, panel (a). Dominant percentage contributions from Breit, perturbative triples and QED corrections to the reduced matrix elements, panel (b), and the lifetime of the clock state, panel (c). Dominant contributions from core orbitals to the dipole polarizability, panel (d).



## B. Excitation Energy

The eigen energies obtained from the solution of many-electron Schrodinger equation, Eq. (1), using FSRCC are used to calculate the excitation energies. The excitation energy of a general state  $nl n' l' (2S+1) L_J$  is defined as

$$\Delta E_{nl n' l' (2S+1) L_J} = E_{nl n' l' (2S+1) L_J} - E_{ns^2 {}^1S_0}, \quad (10)$$

where  $E_{ns^2 {}^1S_0}$  and  $E_{nl n' l' (2S+1) L_J}$  are the exact energies of the ground and excited states, respectively. In Table II, we have listed the excitation energies from our calculations along with other theoretical and experimental data for comparison. To account for *valence-valence* correlations more accurately, we have also included  $6p^2$ ,  $6s6d$  and  $6s7s$  configurations in the model space. For a quantitative assessment of electron correlations, we have listed the contributions from Breit and QED corrections separately.

As evident from the table, our computed energies are in excellent agreement with the experimental results. The largest relative error in our calculation is  $\approx 0.9\%$ , which corresponds to the  ${}^3P_0^o$  state. However, for other states, specially for those which contribute to the lifetime of the clock state, the errors are much smaller. The states  ${}^3P_1^o$ ,  ${}^1P_1^o$ ,  ${}^3S_1$  and  ${}^3D_1$ , which couple either via E1 or M1 operator in the clock transition, have the relative errors of 0.06%, 0.13%, 0.07% and -0.10%, respectively. This is crucial, as these energies contribute to the lifetime of the clock state. Among all the previous theoretical results listed in the table, Ref. [37] is close to ours in terms of the many-body methods used, however, with an important difference. Ref. [37] uses a *linearized* CCSD method, whereas the present work employs a *nonlinear* CCSD, which accounts for electron correlation effects more accurately in the calculation. The relative errors in the reported excitation energies for  ${}^3P_1^o$ ,  ${}^1P_1^o$ ,  ${}^3S_1$  and  ${}^3D_1$  states in Ref. [37] are 1.08%, 0.53%, 0.73% and 0.63%, respectively. Remaining results are mostly based on the multi-configuration Hartree-Fock and its variations and, in general, not consistent in terms of treating electron correlations.

Examining the contributions from high energy configurations, we observed an improvement in the excitation energies of  ${}^3P_1^o$  and  ${}^1P_1^o$  states due to accounting of *valence-valence* correlation more accurately. We find that the relative error has reduced from 0.7% (0.6%) to 0.4% (0.3%) for  ${}^3P_1^o({}^1P_1^o)$  state. Among the contributions from Breit, vacuum polarization and self-energy corrections, the former two are observed to contribute more. The largest cumulative contribution of about 0.3% from Breit and vacuum polarization is observed in the case of  ${}^3P_0^o$ . Self-energy contributions are of opposite phase and negligibly small.

## C. E1 Reduced Matrix Elements

In Table III, we have listed the values of E1 reduced matrix elements from our calculations for all dominant transitions which contribute to the lifetime of the clock state. Since there are more data on oscillator strengths in the literature,

we have converted E1 reduced matrix elements to oscillator strength, and tabulated in the table for comparison with experiments and other theoretical results. The contributions from Breit+QED and triples are provided separately in the table. As evident from the table and as to be expected, DC-CCSD is the dominant contribution to all the matrix elements. The contributions from Breit, QED and perturbative triples are important to obtain accurate results. A quantitative analysis is presented later in the section.

From the literature we could find two previous works, Refs. [19]-CI+MBPT and [37]-CI+all-order, for comparison of the E1 reduced matrix elements. The values of our E1 reduced matrix elements are slightly smaller than Refs. [19] and [37] for all the listed transitions. The reason for this could be attributed to the different treatment of electron correlations in these methods. In Ref. [19], MBPT is used to treat *core-core* and *core-valence* correlations, whereas *valence-valence* correlation is incorporated with CI. In Ref. [37], however, the *core-core* and *core-valence* correlations are accounted using a *linearized* CCSD method. The present work, however, employs a *nonlinear* CCSD theory to account for the *core-core* and *core-valence* correlations and, therefore, is more accurate. The *valence-valence* correlation is however treated in the same way as in Refs. [19, 37]. The other two important inclusions in the present work are, the use of energetically higher configurations ( $6p^2$ ,  $6s7s$  and  $6s6d$ ) in the model space and the corrections from the Breit, QED and perturbative triples.

For the oscillator strength, there are several results in the literature from the previous studies for the  $\langle {}^1S_0 || D || {}^3P_1^o \rangle$  and  $\langle {}^1S_0 || D || {}^1P_1^o \rangle$  transitions for comparison. As evident from the table, there is, however, a large variation in the reported values. For example, for the  $\langle {}^1S_0 || D || {}^3P_1^o \rangle$  transition, the lowest result  $5.44 \times 10^{-2}$  from Ref. [39] differs by  $\approx 33\%$  from the highest result  $8.11 \times 10^{-2}$  reported in the Ref [37]. A similar trend is also observed for the  $\langle {}^1S_0 || D || {}^1P_1^o \rangle$  transition. The lowest value, 1.24 [42], is close to half the highest value, 2.45 [41]. The reason for the large variation could be attributed to the different many-body methods employed in these calculations. It is to be noted that, none of the previous calculations use FSRCC theory, like in the present work. Except Ref. [37], which uses CI + all-order, the other calculations are mostly based on the MCDF and its variations. The large difference among the results clearly indicates the inherent dependence of the results on the choice of configurations in the MCDF method to incorporate electron correlation effects. For the  $\langle {}^1S_0 || D || {}^3P_1^o \rangle$  transition, our result,  $5.46 \times 10^{-2}$ , lies within the range of the previous results. Whereas, for  $\langle {}^1S_0 || D || {}^1P_1^o \rangle$  transition, our result, 1.10, is lowest among all the results listed in the table.

From experiments, to the best of our knowledge, there is one result each for oscillator strength for  $\langle {}^1S_0 || D || {}^3P_1^o \rangle$  [43] and  $\langle {}^1S_0 || D || {}^1P_1^o \rangle$  [47] transitions. Both of these experiments use the beam-foil technique to study atomic spectra. For  $\langle {}^1S_0 || D || {}^3P_1^o \rangle$  transition, our calculated result,  $5.46 \times 10^{-2}$ , has the same order of magnitude as the experimental result,  $(7.3 \pm 0.5) \times 10^{-2}$ , but about 25% smaller. Among the previous theory calculations, the MCDF calculations Refs. [42] and [45] are closer to the experiment. For  $\langle {}^1S_0 || D || {}^1P_1^o \rangle$  tran-

TABLE II. The energy of ground state  $^1S_0$  ( $\text{cm}^{-1}$ ) and excitation energies of some low lying excited states of  $\text{Pb}^{2+}$ . For quantitative analysis of electron correlations, contributions from Breit and QED corrections are given separately.

States	DC-CCSD	Breit	Self-energy	Vac-pol	Total	Other cal.	NIST[36]	% Error
$6s^2\ ^1S_0$	599355.44	12.00	-0.67	188.97	599556	600984[37]	598942	0.1
$6s6p\ ^3P_0^o$	59624.80	121.57	-0.58	81.41	59827	61283[37], 60653[38]	60397	0.94
$6s6p\ ^3P_1^o$	64146.99	116.92	-0.53	82.84	64346	65089[37], 65683[39] 60387[40], 58905[41] 64609[38]	64391	0.06
$6s6p\ ^3P_2^o$	79478.69	83.67	-0.33	90.27	79652	80029[37], 79024[38]	78985	-0.8
$6s6p\ ^1P_1^o$	95045.89	83.07	-0.63	84.30	95213	95847[37], 97970[39] 91983[40], 95537[41] 95535[38]	95340	0.13
$6p^2\ ^3P_0$	142922.33	236.01	-1.41	169.97	143327	143571[37]	142551	-0.54
$6s7s\ ^3S_1$	149898.62	4.90	-0.32	64.10	149967	151183[37]	150084	0.07
$6s6d\ ^1D_2$	152651.06	108.27	-0.70	135.00	152894	153614[37]	151885	-0.6
$6s7s\ ^1S_0$	153901.92	3.47	-0.28	62.88	153968	155054[37]	153783	-0.12
$6p^2\ ^3P_1$	155401.22	189.27	-1.16	170.87	155760	156610[37]	155431	-0.2
$6s6d\ ^3D_1$	157523.12	17.37	-0.55	92.43	157632	158439[37]	157444	-0.1
$6s6d\ ^3D_2$	157902.47	5.93	-0.48	87.81	157996	159134[37]	157925	-0.04
$6s6d\ ^3D_3$	159147.60	0.04	-0.38	86.03	159233	160530[37]	158957	-0.17
$6p^2\ ^3P_2$	164987.49	117.07	-0.99	143.34	165247	165898[37]	164818	-0.26
$6p^2\ ^1D_2$	179412.09	139.08	-1.17	166.70	179717	179646[37]	178432	-0.7
$6p^2\ ^1S_0$	189714.06	161.46	-1.17	179.67	190054	190061[37]	188615	-0.7

<sup>a</sup> Ref. [37] - CI + all-order, <sup>b</sup> Ref. [38] - MCDHF, <sup>c</sup> Ref. [39] - CIRHF + CP, <sup>d</sup> Ref. [40] - CIRHF + CP, <sup>e</sup> Ref. [41] - MCRRPA

TABLE III. The E1 and M1 reduced matrix elements (a.u.) and oscillator strengths for some allowed transitions in  $\text{Pb}^{2+}$ . For comparison, data from experiments and other theory calculations are also provided.

States	DC-CCSD	Breit + QED	P-triples	Total	Other cal.	Expt.
E1 Reduced Matrix Elements						
$\langle ^1S_0    D    ^3P_1^o \rangle$	0.5319	-0.0007	-0.0024	0.5288	0.706[19], 0.644[37]	
$\langle ^1S_0    D    ^1P_1^o \rangle$	1.9854	0.0003	-0.0327	1.9530	2.350[19], 2.384[37]	
$\langle ^3S_1    D    ^3P_0^o \rangle$	0.5362	0.0120	-0.0123	0.5359	0.963[37]	
$\langle ^3D_1    D    ^3P_0^o \rangle$	-1.4796	0.0171	-0.0355	-1.4980	-1.516[37]	
Oscillator Strengths						
$\langle ^1S_0    D    ^3P_1^o \rangle$	5.5071[-2]	0.0026[-2]	-0.4950[-2]	5.4602[-2]	8.11[-2][37], 7.40[-2][42], 5.44[-2][39], 7.55[-2][45], 6.15[-2][41], 6.15[-2][46] 5.52[-2][40]	(7.3 ± 0.5)[-2][43], [44]
$\langle ^1S_0    D    ^1P_1^o \rangle$	1.1369	0.0023	-0.0371	1.1021	1.65[37], 1.24[42], 1.64[39], 1.51[45], 2.45[41], 1.42[46], 1.43[40]	(1.01 ± 0.20)[47]
$\langle ^3S_1    D    ^3P_0^o \rangle$	0.0788	0.0034	-0.0036	0.0786	0.229[42]	
$\langle ^3D_1    D    ^3P_0^o \rangle$	0.6504	-0.0156	0.0315	0.6663	0.93[42]	
M1 Reduced Matrix Elements						
$\langle ^3P_1^o    M1    ^3P_0^o \rangle$	-1.3117	-0.0005	0.0006	-1.3116	-0.674[19]	
$\langle ^1P_1^o    M1    ^3P_0^o \rangle$	0.4972	0.0002	0.0001	0.4975	0.205[19]	
$\langle ^1S_0    M1    ^3S_1 \rangle$	0.0044	-0.0003	0	0.0041		
$\langle ^1S_0    M1    ^3D_1 \rangle$	-0.0143	-0.003	0.0004	-0.0169		

<sup>a</sup> Ref. [19] - CI + MBPT, <sup>b</sup> Ref. [42] - IC + RHF + CP, <sup>c</sup> Ref. [45] - CIDF - MP, <sup>d</sup> Ref. [46] - MCRRPA, <sup>e</sup> Ref. [37] - CI + all-order, <sup>f</sup> Ref. [48] - IC + RHF, <sup>g</sup> Ref. [40] - CIRHF + CP, <sup>h</sup> Ref. [41] - MCRRPA, <sup>i</sup> Ref. [39] - CIRHF + CP,

TABLE IV. Termwise contributions to E1 and M1 reduced matrix elements (a.u.) from different terms in FSRCC theory. The operator  $\hat{O}$  represents the electric or magnetic dipole operator.

Terms + h. c.	$\langle {}^1S_0    \hat{D}    {}^1P_1^o \rangle$	$\langle {}^3P_1^o    \hat{M}1    {}^3P_0^o \rangle$
DF	2.1575	-1.3586
1v diagrams	-0.4014	-0.0122
$\hat{O}R_2$	0.1064	0.0199
$R_2\hat{O}R_2$	0.0735	0.0423
$S_1\hat{O}R_2 + S_2\hat{O}R_2 + S_1^2\hat{O}R_2$	0.0101	-0.0081
$\hat{O}S_2$	0.0065	0.0003
$S_2\hat{O}S_2 + S_2\hat{O}S_1 + S_2\hat{O}S_1^2$	0.0320	0.0046
$T_1\hat{O}R_2$	-0.0001	0
$S_2\hat{O}T_2 + S_2\hat{O}T_1$	0.0007	0
$T_2\hat{O}T_2 + T_1\hat{O}T_2$	0.0003	0
Total	1.9855	-1.3118

sition, however, among all the theory results listed in table, our result, 1.10, has the best match with the experimental result,  $1.01 \pm 0.20$  [47].

#### D. M1 Reduced Matrix Elements

For the clock transition, the theoretical estimate of the M1 matrix elements is the other important component to calculate the lifetime of the clock state. So, we next compute the M1 reduced matrix elements of the transitions which contribute dominantly to  $\tau$ . These are listed in the Table III. As to be expected, like the case of E1 matrix elements, the most dominant contribution is from DC-CCSD for all the transitions. The cumulative contribution from Breit, QED and perturbative triples are small but important to get reliable transition properties results.

Unlike the E1 matrix elements, only few results of M1 are available in the literature for comparison. To the best of our knowledge, there is only one theoretical result calculated using CI+MBPT [19], which reports the values of M1 reduced matrix elements for the  $\langle {}^3P_1^o || \hat{M}1 || {}^3P_0^o \rangle$  and  $\langle {}^1P_1^o || \hat{M}1 || {}^3P_0^o \rangle$  transitions. Interestingly, unlike the E1 reduced matrix elements where the two works are comparable, our results for M1 reduced matrix elements differ by a factor of two or more from Ref. [19]. This leads to a difference of  $\approx 6.7\%$  between the lifetimes calculated using the two data. Our calculated value of  $\tau$  with  $6s^2+6s6p$  configuration is  $9.6 \times 10^6$  s, whereas the value reported in Ref. [19] is  $9.0 \times 10^6$  s. As this work reports our first implementation and computation of M1 matrix element for two-valence system using FSRCC, it is essential to cross check and validate our results with previous works. For this we compute and compare the results of other atoms since there are no previous theoretical or experimental results for  $\text{Pb}^{2+}$  other than Ref. [19]. In particular, we consider the M1 transition rate for the  $\langle {}^3P_2^o || \hat{M}1 || {}^3P_1^o \rangle$  transition in neutral Yb. This was studied in Ref. [6], using a combined method of configuration interaction (CI) and perturbation the-

ory (PT), and reported a value as  $6.7 \times 10^{-2} \text{ s}^{-1}$ . And from our implementation we obtain  $5.3 \times 10^{-2} \text{ s}^{-1}$ . Reason for this small difference could be attributed to the better consideration of electron correlations in FSRCC theory. In another work Ref. [49] the transition rate for  $\langle {}^3P_2^o || \hat{M}1 || {}^3P_1^o \rangle$  of Sr was computed using CI+RPA. It reported the value as  $8.26 \times 10^{-4}$ , this matches very well with our result of  $8.88 \times 10^{-4}$ . The difference is only 7% which could again be due to better accounting of electron correlations in FSRCC. In yet another seminal work, Ref. [50] carried out a second-order MBPT calculation of M1 reduced matrix elements for  $\langle {}^3P_0^o || \hat{M}1 || {}^3P_1^o \rangle$  and  $\langle {}^3P_0^o || \hat{M}1 || {}^1P_1^o \rangle$  transitions in  $\text{Fe}^{22+}$ . The reported values, 1.40 and 0.22, respectively are in good agreement with our computed values, 1.37 and 0.28. Thus, from all the comparison with the previous theoretical results for different systems, we can infer that our implementation of M1 matrix element computation with FSRCC gives reliable results.

#### E. Lifetime of Clock State

The lifetime of the clock state can now be theoretically estimated using the results discussed above. Using the E1 and M1 reduced matrix elements listed in Table III and excitation energies from Table II in Eq. (7), we obtain the E1M1 decay rate ( $\Gamma$ ) for the  $6s^2 {}^1S_0 \rightarrow 6s6p {}^3P_0^o$  clock transition and its inverse is  $\tau$ . The  $\tau$  obtained from our calculations is given in the Table V. To assess the effect of *valence-valence* correlation, we have separated the contributions from  $6s6p$ ,  $6s7s$  and  $6s6d$  configurations. Our computed lifetime,  $9.76 \times 10^6$  s, is  $\approx 8.5\%$  larger than the only other theoretical result [19]. The reason for this could be attributed to the more accurate treatment of electron correlations in our calculations. It should be noted that, our calculations also incorporate the contributions from E1 and M1 matrix elements from higher energy states  $6s6d {}^3D_1$  and  $6s7s {}^3S_1$ . This has a significant cumulative contribution of  $\approx 3.3\%$  to the total lifetime. The other key difference from Ref. [19] is, the inclusion of the corrections from Breit, QED and perturbative triples in our calculations. The contribution from the perturbative triples is  $\approx -2.3\%$  to the lifetime. This is consistent with the trend observed in our previous work on  $\text{Al}^+$  atomic clock [16]. The contributions from the Breit and QED corrections are also significant, they jointly contribute  $\approx 1.1\%$  of the total  $\tau$ . As discernible from the Fig. 4(c), the DF alone contributes  $\approx 33\%$  of the total value. The most significant contribution arises from the electron correlations associated with the residual Coulomb interaction through FSRCC within the CCSD framework. The combined contribution from DF and CCSD is about 101% of the total lifetime.

#### F. Dipole Polarizability

The electric dipole polarizability,  $\alpha$ , of an atom or ion is a measure of the response to an external electric field. It is related to properties which serve as signatures of several fundamental properties [5, 51, 52]. In the present work,  $\alpha$  is

TABLE V. The lifetime of the clock state  $^3P_0^o$ . The contributions from the Breit, QED and perturbative triples corrections are provided separately.

Configurations/Methods	$\tau (\times 10^6 \text{ s})$
$6s^2 + 6s6p$	9.595
$6s7s$	0.029
$6s6d$	0.248
Total CCSD	9.872
CCSD(T)	9.654
CCSD(T)+Breit+QED	9.761
Recommended	$(9.76 \pm 0.47)$
Others	9.0[19]

TABLE VI. The value of  $\alpha$  (a.u.) for ground state,  $6s^2 \ ^1S_0$ , of  $\text{Pb}^{2+}$  from PRCC calculation. The available data from experiment and other theory calculations are also provided for comparison.

State	Present work	
	Method	$\alpha$
$6s^2 \ ^1S_0$	DF	16.246
	PRCC	14.173
	PRCC(T)	14.166
	PRCC(T)+Breit	14.173
	PRCC(T)+Breit+QED	14.064
	Estimated	14.016
	Recommended	$14.02 \pm 0.21$
	Other cal.	$13.3 \pm 0.4^a$
	Expt.	$13.62 \pm 0.08^b$

<sup>a</sup>Ref.[37]-CI + all-order, <sup>b</sup>Ref.[53]-Expt.

required in calculating the BBR shift of the clock transition frequency. In the Table VI, we present our theoretical result on  $\alpha$  for the ground state of  $\text{Pb}^{2+}$  and compare it with results available in the literature. To calculate  $\alpha$ , we have used the PRCC theory developed and presented in our previous works [23, 27]. The Table VI also list the contributions from various correlation terms subsumed in the PRCC theory. The term *estimated* identifies the contribution from the orbitals from  $i$ ,  $j$  and  $k$ -symmetries. As to be expected, the dominant contribution is from the DF term. It contributes  $\approx 116\%$  of the total value. The PRCC value is  $\approx 13\%$  lower than the DF value. The reason for this is the cancellation due to opposite contributions from electron correlation.

From the literature, we could find one result each from the experimental and theoretical studies. On comparing the results, our recommended value, 14.02, is in good agreement with the experimental value,  $13.62 \pm 0.08$ , reported in Ref. [53]. The difference from the experimental result is  $\approx 3\%$ . In theoretical work of Safronova and collaborators [37], the reported value of 13.3 is obtained using the CI+all-order method. Our recommended result is  $\approx 6\%$  larger than Ref. [37]. As mentioned earlier, reason for this difference could be attributed to the more accurate treatment of electron correlations in the present calculation. The other important

TABLE VII. Termwise contributions to  $\alpha$  (a.u.) from different terms in PRCC theory.

Terms + h. c.	$\alpha$
$\mathbf{T}_1^{(1)\dagger} \mathbf{D}$	16.6849
$\mathbf{T}_1^{(1)\dagger} \mathbf{D} \mathbf{T}_2^{(0)}$	-1.0835
$\mathbf{T}_1^{(1)\dagger} \mathbf{D} \mathbf{T}_1^{(0)}$	-0.2746
$\mathbf{T}_2^{(1)\dagger} \mathbf{D} \mathbf{T}_1^{(0)}$	-0.0052
$\mathbf{T}_2^{(1)\dagger} \mathbf{D} \mathbf{T}_2^{(0)}$	0.4145
Normalization	-1.5633
Total	14.1733

advantage of the present calculation is that, it does not employ the sum-over-state approach [54, 55] to incorporate the effects of perturbation. The summation over all the possible intermediate states is accounted through the perturbed cluster operators [16, 23]. In addition, the present work also incorporates the effects of Breit, QED and perturbative triples corrections in the calculation of  $\alpha$ .

### G. Electron Correlations in FSRCC and PRCC Theories and Corrections from Breit, QED and Perturbative Triples

To get insights on the correlation effects, we now analyze and present the trend of contributions from various correlation terms in FSRCC and PRCC theories as well as the contributions from the Breit and QED corrections. As mentioned earlier, the FSRCC method is used to calculate the lifetime of the metastable clock state, whereas PRCC theory is employed to calculate  $\alpha$  for the ground state of  $\text{Pb}^{2+}$ .

In Table IV, we have listed the term-wise contributions from FSRCC for selected E1 and M1 matrix elements. As expected, the DF is the leading order (LO) term for both the matrix elements. It contributes  $\approx 109$  and  $104\%$  of the total value for  $\langle ^1S_0 || D || ^1P_1^o \rangle$  and  $\langle ^3P_1^o || M1 || ^3P_0^o \rangle$ , respectively. The next leading order (NLO) contribution of the two matrix elements show different trends. For  $\langle ^1S_0 || D || ^1P_1^o \rangle$ , the NLO contribution of opposite phase of  $\approx -20\%$  arises from the *one-valence* sector. Whereas, for  $\langle ^3P_1^o || M1 || ^3P_0^o \rangle$ , the NLO contribution is from the *two-valence* sector, the  $R_2 \hat{O} R_2$  term gives a contribution of  $\approx -3\%$ . As the next dominant contribution, the term  $\hat{O} R_2 + \text{h.c.}$  contributes  $\approx 5$  and  $1.5\%$ , respectively, to  $\langle ^1S_0 || D || ^1P_1^o \rangle$  and  $\langle ^3P_1^o || M1 || ^3P_0^o \rangle$  matrix elements.

For the contributions from the Breit and QED corrections to matrix elements, the largest contribution is observed in the case of  $\langle ^1S_0 || M1 || ^3D_1 \rangle$  transition. The Breit contributes  $\approx 13.0\%$ , whereas the contribution from the QED is  $\approx 5.0\%$  of the total value. transition. The largest contribution from the perturbative triples is observed to be  $\approx 2.4\%$ , in the case of  $\langle ^3D_1 || D || ^3P_0^o \rangle$ . Combining these two, the largest consolidated contribution from Breit+QED+perturbative triples is  $\approx 20\%$ . Considering the high accuracies associated with atomic clocks, this is a significant contribution. Hence, it is impor-



tant to include these to obtain reliable clock properties from theoretical calculations.

To understand the nature of electron correlations subsumed in computations of  $\alpha$ , we have listed the termwise contributions from PRCC theory in Table VII. As evident from the table, the LO term,  $\mathbf{T}_1^{(1)\dagger}\mathbf{D} + \text{h. c.}$ , contributes  $\approx 118\%$  of the total value. This is expected, as it includes the DF and dominant contribution from *core-polarization*. For a better illustration, in Fig. 4(d), we have shown the five dominant contributions from core orbitals. As discernible from the figure,  $\approx 87\%$  of the LO contribution arises from the  $6s$  valence-electrons through the dipolar mixing with the  $6p$  states. This is due to the larger radial extent of the  $6s$  orbital. In the remaining LO contribution, a contribution of  $\approx 8.5\%$  is from the  $5d$  core-electrons, through the dipolar mixing with  $6p$  and  $4f$ -electrons. The NLO term is  $\mathbf{T}_1^{(1)\dagger}\mathbf{D}\mathbf{T}_2^{(0)}$ , it contributes  $\approx 8\%$ . It is to be noted that, it accounts for the dominant *pair-correlation* effects through the  $\mathbf{T}_2^{(0)}$  operator. The next dominant contribution of  $\approx 3\%$ , which also include some part of *pair-correlation*, is from  $\mathbf{T}_2^{(1)\dagger}\mathbf{D}\mathbf{T}_2^{(0)}$ .

The perturbative triples and Breit each contributes  $\approx 0.04\%$  to  $\alpha$ . The contribution from QED is, however, significant,  $\approx 0.7\%$ . So, the cumulative contribution from Breit+QED+perturbative triples is  $\approx 0.8\%$ . The contribution from the higher symmetry orbitals is estimated to be  $\approx 0.34\%$  of the total value.

## V. THEORETICAL UNCERTAINTY

The theoretical uncertainty in the computed  $\tau$  depends on the uncertainties in the E1 and M1 matrix elements and the energy denominators, as they contribute in Eq. (7). As the experimental results are not available for all the E1 and M1 reduced matrix elements, we have identified four different sources which can contribute to the uncertainty in E1 and M1 matrix elements. The first source of uncertainty is due to the truncation of the basis set in our calculation. As discussed in the basis convergence section, our calculated values of E1 and M1 reduced matrix elements converge to the order of  $10^{-3}$  or smaller with basis. Since this is a very small change, we may neglect this uncertainty. The second source of uncertainty arises from the truncation of the dressed Hamiltonian  $\tilde{H}_{\text{hfs}}^e$  at the second order of  $T^{(0)}$  in the properties calculation. In our earlier work [29], using an iterative scheme, we found that the terms with third and higher orders in  $T^{(0)}$  contribute less than  $0.1\%$ . So, we consider  $0.1\%$  as an upper bound for this source. The third source is due to the partial inclusion of triple excitations in the properties calculation. Since the perturbative triples account for the leading order terms of triple excitation, the contribution from remaining terms will be small. Based on the analysis from our previous works [23, 56] we estimate the upper bound from this source as  $0.72\%$ . The fourth source of uncertainty could be associated with the frequency-dependent Breit interaction which is not included in the present calculations. However, in our previous work [57], using a series of computations using GRASP2K we estimated an upper bound

on this uncertainty as  $0.13\%$  in Ra. So, for the present work, we take  $0.13\%$  as an upper bound from this source. There could be other sources of theoretical uncertainty, such as the higher order coupled perturbation of vacuum polarization and self-energy terms, quadruply excited cluster operators, etc. However, in general, these all have much lower contributions to the properties and their cumulative theoretical uncertainty could be below  $0.1\%$ . Uncertainty in the energy denominator is estimated using the relative errors in the energy difference of  $^3P_1^o$ ,  $^1P_1^o$ ,  $^3S_1$  and  $^3D_1$  intermediate states with respect to  $^3P_0^o$ . Among all the intermediate states,  $^1P_1^o$  and  $^3D_1$  states contribute dominantly, through routes 1 and 2, respectively, to the lifetime. The relative errors in the energy difference of these states with  $^3P_0^o$  are  $1.27\%$  and  $0.78\%$ , respectively. Since they correspond to the dominant contributions, we have taken them as the uncertainty in the energy denominator. By combining the upper bounds of all the uncertainties, the theoretical uncertainty associated with the lifetime of the clock state is  $\approx 4.8\%$ . It should, however, be noted that the uncertainty in the value of  $\alpha$  is much smaller, about  $1.5\%$  [58]

## VI. CONCLUSIONS

We have employed an all-particle multireference Fock-space relativistic coupled-cluster theory to examine the clock transition properties in  $\text{Pb}^{2+}$ . We have computed the excitation energies of several low lying states, and the E1 and M1 transition amplitudes for all the allowed transitions within the model space considered. These are then used to calculate the lifetime of the clock state. Moreover, using PRCC theory, we also calculated the electric dipole polarizability for the ground state of  $\text{Pb}^{2+}$ . In all these calculations, to obtain accurate properties results, we incorporate the corrections from the relativistic and QED effects. The dominant contribution from triple excitations is incorporated though perturbative triples and a fairly large basis sets is used to achieve the convergence of the properties.

Our computed excitation energies are in excellent agreement with experimental values for all the states. Our result of  $\tau$  is about  $8.5\%$  larger than the previous result obtained using CI+MBPT [19]. The reason for the higher  $\tau$  in the present calculation could partially be attributed to the better inclusion of *core-core* and *core-valence* electron correlations in the FS-RCC theory. In addition, to account for the *valence-valence* correlation more accurately, we also incorporated the contributions from the higher energy configurations  $6s6d$  and  $6s7s$  in our calculation. Based on our analysis, we find that this contributes  $\approx 3.3\%$  of the total lifetime. In addition, from our study, we find that the contributions from the perturbative triples and Breit+QED corrections are crucial to get reliable  $\tau$ . They are observed to contribute  $\approx -2.2\%$  and  $1.1\%$ , respectively. Our recommended value of dipole polarizability is in good agreement with the available experimental value, with a small difference of  $\approx 3\%$ . Based on our analysis on theoretical uncertainty, the upper bound on uncertainty for calculated lifetime is  $\approx 4.8\%$ , whereas for polarizability it is  $\approx 1.5\%$ .

TABLE VIII. Convergence trend of  $\alpha$ , and E1 and M1 matrix elements as a function of basis size.

Basis	$\alpha$	$\langle {}^1S_0    D    {}^1P_1^o \rangle$	$\langle {}^3P_1^o    M1    {}^3P_0^o \rangle$
96 : 20s15p12d7f4g0h	15.919	2.0512	1.3158
103 : 19s16p13d8f3g2h	15.660	2.0268	1.3153
114 : 20s17p14d9f4g3h	14.979	1.9966	1.3198
125 : 21s18p15d10f5g4h	14.467	1.9873	1.3134
136 : 22s19p16d11f6g5h	14.274	1.9888	1.3126
147 : 23s20p17d12f7g6h	14.205	1.9883	1.3121
158 : 24s21p18d13f8g7h	14.175	1.9875	1.3118
169 : 25s22p19d14f9g8h	14.173	1.9854	1.3117

## ACKNOWLEDGMENTS

The authors wish to thank Suraj Pandey for the useful discussion. Palki acknowledges the fellowship sup-

port from UGC (BININ04154142), Govt. of India. B. K. M acknowledges the funding support from SERB, DST (CRG/2022/003845). Results presented in the paper are based on the computations using the High Performance Computing clusters Padum at IIT Delhi and PARAM HIMALAYA facility at IIT Mandi under the National Supercomputing Mission of Government of India.

## Appendix A: Convergence of $\alpha$ and E1 and M1 matrix elements

In Table VIII, we provide the trend of the convergence of dipole polarizability and E1 and M1 matrix elements as a function of the basis size. As it is evident from the table, all the properties converge to the order of  $10^{-3}$  or less in the respective units of the properties.

- 
- [1] A. D. Ludlow, M. M. Boyd, J. Ye, E. Peik, and P. O. Schmidt, “Optical atomic clocks,” *Rev. Mod. Phys.* **87**, 637–701 (2015).
  - [2] S. De and A. Sharma, “Indigenisation of the Quantum Clock: An Indispensable Tool for Modern Technologies,” *Atoms* **11**, 71 (2023).
  - [3] M. S. Safronova, “The search for variation of fundamental constants with clocks,” *Annalen der Physik* **531**, 1800364 (2019).
  - [4] J. D. Prestage, R. L. Tjoelker, and L. Maleki, “Atomic clocks and variations of the fine structure constant,” *Phys. Rev. Lett.* **74**, 3511–3514 (1995).
  - [5] S. G. Karshenboim and E. Peik, *Astrophysics, Clocks and Fundamental Constants, Lecture Notes in Physics* (Springer, New York, 2010).
  - [6] V. A. Dzuba, V. V. Flambaum, and S. Schiller, “Testing physics beyond the standard model through additional clock transitions in neutral ytterbium,” *Phys. Rev. A* **98**, 022501 (2018).
  - [7] J. C. Berengut, D. Budker, C. Delaunay, V. V. Flambaum, C. Fruguele, E. Fuchs, C. Grojean, Roni Harnik, R. Ozeri, G. Perez, and Y. Soreq, “Probing new long-range interactions by isotope shift spectroscopy,” *Phys. Rev. Lett.* **120**, 091801 (2018).
  - [8] M. S. Grewal, A. P. Andrews, and C. G. Bartone, *Global Navigation Satellite Systems, Inertial Navigation, and Integration* (John Wiley and Sons, New York, 2013).
  - [9] F.G. Major, *The Quantum Beat: The Physical Principles of Atomic Clocks* (Springer New York, 2013).
  - [10] D. S. Weiss and M. Saffman, “Quantum computing with neutral atoms,” *Physics Today* **70**, 44–50 (2017).
  - [11] D. J. Wineland, J. C. Bergquist, J. J. Bollinger, R. E. Drullinger, and W. M. Itano, “Quantum computers and atomic clocks,” in *Frequency Standards and Metrology* (2002) pp. 361–368.
  - [12] F. Riehle, P. Gill, F. Arias, and L. Robertsson, “The CIPM list of recommended frequency standard values: guidelines and procedures,” *Metrologia* **55**, 188 (2018).
  - [13] S. M. Brewer, J.-S. Chen, A. M. Hankin, E. R. Clements, C. W. Chou, D. J. Wineland, D. B. Hume, and D. R. Leibbrandt, “ ${}^{27}\text{Al}^+$  quantum-logic clock with a systematic uncertainty below  $10^{-18}$ ,” *Phys. Rev. Lett.* **123**, 033201 (2019).
  - [14] M. Kállay, H. S. Nataraj, B. K. Sahoo, B. P. Das, and L. Visscher, “Relativistic general-order coupled-cluster method for high-precision calculations: Application to the  $\text{Al}^+$  atomic clock,” *Phys. Rev. A* **83**, 030503 (2011).
  - [15] M. S. Safronova, M. G. Kozlov, and C. W. Clark, “Precision Calculation of Blackbody Radiation Shifts for Optical Frequency Metrology,” *Phys. Rev. Lett.* **107**, 143006 (2011).
  - [16] R. Kumar, S. Chattopadhyay, D. Angom, and B. K. Mani, “Fock-space relativistic coupled-cluster calculation of a hyperfine-induced  ${}^1S_0 \rightarrow {}^3P_0^o$  clock transition in  $\text{Al}^+$ ,” *Phys. Rev. A* **103**, 022801 (2021).
  - [17] T. Nicholson, S. Campbell, R. Hutson, E. Marti, B. Bloom, R. McNally, W. Zhang, M. Barrett, M. Safronova, G. Strouse, W. Tew, and J. Ye, “Systematic evaluation of an atomic clock at  $2 \times 10^{-18}$  total uncertainty,” *Nature Communications* **6**, 6896 (2015).
  - [18] T. Bothwell, D. Kedar, E. Oelker, J. Robinson, S. Bromley, W. Tew, Ju. Ye, and C. Kennedy, “JILA Sr I optical lattice clock with uncertainty of  $2.0 \times 10^{-18}$ ,” *Metrologia* **56**, 065004 (2019).
  - [19] K. Belay, “Prospects of a  $\text{Pb}^{2+}$  ion clock,” *Phys. Rev. Lett.* **127**, 013201 (2021).
  - [20] R. Pal, M. S. Safronova, W. R. Johnson, A. Derevianko, and S. G. Porsev, “Relativistic coupled-cluster single-double method applied to alkali-metal atoms,” *Phys. Rev. A* **75**, 042515 (2007).
  - [21] B. K. Mani, K. V. P. Latha, and D. Angom, “Relativistic coupled-cluster calculations of  ${}^{20}\text{Ne}$ ,  ${}^{40}\text{Ar}$ ,  ${}^{84}\text{Kr}$ , and  ${}^{129}\text{Xe}$ : Correlation energies and dipole polarizabilities,” *Phys. Rev. A* **80**, 062505 (2009).
  - [22] H. S. Nataraj, B. K. Sahoo, B. P. Das, and D. Mukherjee, “Reappraisal of the electric dipole moment enhancement factor for thallium,” *Phys. Rev. Lett.* **106**, 200403 (2011).
  - [23] R. Kumar, S. Chattopadhyay, B. K. Mani, and D. Angom, “Electric dipole polarizability of group-13 ions using perturbed relativistic coupled-cluster theory: Importance of nonlinear terms,” *Phys. Rev. A* **101**, 012503 (2020).
  - [24] E. Eliav, U. Kaldor, and Y. Ishikawa, “Transition energies of ytterbium, lutetium, and lawrencium by the relativistic coupled-cluster method,” *Phys. Rev. A* **52**, 291–296 (1995).
  - [25] E. Eliav, U. Kaldor, and Y. Ishikawa, “Transition energies of mercury and ekamercury (element 112) by the relativistic coupled-cluster method,” *Phys. Rev. A* **52**, 2765–2769 (1995).

- [26] B. K. Mani and D. Angom, “Fock-space relativistic coupled-cluster calculations of two-valence atoms,” *Phys. Rev. A* **83**, 012501 (2011).
- [27] R. Kumar, S. Chattopadhyay, D. Angom, and B. K. Mani, “Relativistic coupled-cluster calculation of the electric dipole polarizability and correlation energy of Cn,  $\text{Nh}^+$ , and Og: Correlation effects from lighter to superheavy elements,” *Phys. Rev. A* **103**, 062803 (2021).
- [28] B.K. Mani, S. Chattopadhyay, and D. Angom, “RCCPAC: A parallel relativistic coupled-cluster program for closed-shell and one-valence atoms and ions in fortran,” *Computer Physics Communications* **213**, 136–154 (2017).
- [29] B. K. Mani and D. Angom, “Atomic properties calculated by relativistic coupled-cluster theory without truncation: Hyperfine constants of  $\text{Mg}^+$ ,  $\text{Ca}^+$ ,  $\text{Sr}^+$ , and  $\text{Ba}^+$ ,” *Phys. Rev. A* **81**, 042514 (2010).
- [30] D.P. Craig and T. Thirunamachandran, *Molecular Quantum Electrodynamics: An Introduction to Radiation-molecule Interactions*, Dover Books on Chemistry Series (Dover Publications, 1998).
- [31] R. Santra, K. V. Christ, and Ch. H. Greene, “Properties of metastable alkaline-earth-metal atoms calculated using an accurate effective core potential,” *Phys. Rev. A* **69**, 042510 (2004).
- [32] A. K. Mohanty, F. A. Parpia, and E. Clementi, “Kinetically balanced geometric gaussian basis set calculations for relativistic many-electron atoms,” in *Modern Techniques in Computational Chemistry: MOTECC-91*, edited by E. Clementi (ESCOM, 1991).
- [33] P. Jönsson, G. Gaigalas, J. Bieroń, C. Froese Fischer, and I. P. Grant, “New version: Grasp2k relativistic atomic structure package,” *Comp. Phys. Comm.* **184**, 2197 – 2203 (2013).
- [34] R. E. Stanton and S. Havriliak, “Kinetic balance: A partial solution to the problem of variational safety in dirac calculations,” *J. Chem. Phys.* **81**, 1910–1918 (1984).
- [35] O. Zatsarinny and C. F. Fischer, “DBSR<sub>HF</sub>: A B-spline Dirac-Hartree-Fock program,” *Computer Physics Communications* **202**, 287 – 303 (2016).
- [36] “Nist atomic spectroscopic database,” <https://physics.nist.gov/PhysRefData/ASD/levels.html> (2013).
- [37] M. S. Safronova, M. G. Kozlov, and U. I. Safronova, “Atomic properties of Pb III,” *Phys. Rev. A* **85**, 012507 (2012).
- [38] L. J. Curtis, R. E. Irving, M. Henderson, R. Matulioniene, C. Froese Fischer, and E. H. Pinnington, “Measurements and predictions of the  $6s6p\ ^1P_1$  lifetimes in the Hg isoelectronic sequence,” *Phys. Rev. A* **63**, 042502 (2001).
- [39] J. Migdalek and W. E. Baylis, “Relativistic oscillator strengths and excitation energies for the  $ns^2\ ^1S_0 - nsnp\ ^3P_1, ^1P_1$  transitions in the mercury isoelectronic sequence,” *Journal of Physics B: Atomic and Molecular Physics* **18**, 1533 (1985).
- [40] J Migdalek and A Bojara, “Relativistic CI calculations for the  $ns^2\ ^1S_0 - nsnp\ ^3P_1, ^1P_1$  transitions in the cadmium and mercury isoelectronic sequences,” *Journal of Physics B: Atomic, Molecular and Optical Physics* **21**, 2221 (1988).
- [41] H. S. Chou and K. N. Huang, “Relativistic excitation energies and oscillator strengths for the  $6s^2\ ^1S_0 \rightarrow 6s6p\ ^1P_1, ^3P_1$  transitions in Hg-like ions,” *Phys. Rev. A* **45**, 1403–1406 (1992).
- [42] A. Alonso-Medina, C. Colón, and A. Zanoń, “Core-polarization effects, oscillator strengths and radiative lifetimes of levels in Pb III,” *Monthly Notices of the Royal Astronomical Society* **395**, 567–579 (2009).
- [43] E.H. Pinnington, W. Ansbacher, J.A. Kernahan, Z.-Q. Ge, and A.S. Inamdar, “Beam-foil spectroscopy for ions of lead and bismuth,” *Nuclear Instruments and Methods in Physics Research Section B: Beam Interactions with Matter* **106**, 1–10 (1996).
- [44] W. Ansbacher, E. H. Pinnington, and J. A. Kernahan, “Beam-foil lifetime measurements in Pb III and Pb IV,” *Canadian Journal of Physics* **66**, 402 (1988).
- [45] L. Glowacki and J. Migdalek, “Relativistic configuration-interaction oscillator strength calculations with ab initio model potential wavefunctions,” *Journal of Physics B: Atomic, Molecular and Optical Physics* **36**, 3629 (2003).
- [46] H. S. Chou and K. N. Huang, “Core-shielding effects on photoexcitation of the Hg-like ions,” *Chinese Journal of Physics* **35**, 35–46 (1997).
- [47] T. Andersen, A. Kirkegård Nielsen, and G. Sørensen, “A Systematic Study of Atomic Lifetimes of Levels Belonging to the Ag I, Cd I, Au I, and Hg I Isoelectronic Sequences,” *Physica Scripta* **6**, 122–124 (1972).
- [48] C Colón and A Alonso-Medina, “Determination of theoretical transition probabilities for the Pb III spectrum,” *Physica Scripta* **62**, 132 (2000).
- [49] A. Derevianko, “Feasibility of cooling and trapping metastable alkaline-earth atoms,” *Phys. Rev. Lett.* **87**, 023002 (2001).
- [50] U. I. Safronova, W. R. Johnson, and A. Derevianko, “Relativistic many-body calculations of magnetic dipole transitions in Be-like ions,” *Physica Scripta* **60**, 46 (1999).
- [51] I.B. Khriplovich, *Parity Nonconservation in Atomic Phenomena* (Gordon and Breach Science Publishers, Philadelphia, 1991).
- [52] W. C. Griffith, M. D. Swallows, T. H. Loftus, M. V. Romalis, B. R. Heckel, and E. N. Fortson, “Improved limit on the permanent electric dipole moment of  $^{199}\text{Hg}$ ,” *Phys. Rev. Lett.* **102**, 101601 (2009).
- [53] M. E. Hanni, Julie A. Keele, S. R. Lundeen, C. W. Fehrenbach, and W. G. Sturuss, “Polarizabilities of  $\text{Pb}^{2+}$  and  $\text{Pb}^{4+}$  and ionization energies of  $\text{Pb}^+$  and  $\text{Pb}^{3+}$  from spectroscopy of high- $l$  rydberg states of  $\text{Pb}^+$  and  $\text{Pb}^{3+}$ ,” *Phys. Rev. A* **81**, 042512 (2010).
- [54] M. S. Safronova, W. R. Johnson, and A. Derevianko, “Relativistic many-body calculations of energy levels, hyperfine constants, electric-dipole matrix elements, and static polarizabilities for alkali-metal atoms,” *Phys. Rev. A* **60**, 4476–4487 (1999).
- [55] A. Derevianko, W. R. Johnson, M. S. Safronova, and J. F. Babb, “High-precision calculations of dispersion coefficients, static dipole polarizabilities, and atom-wall interaction constants for alkali-metal atoms,” *Phys. Rev. Lett.* **82**, 3589–3592 (1999).
- [56] S. Chattopadhyay, B. K. Mani, and D. Angom, “Triple excitations in perturbed relativistic coupled-cluster theory and electric dipole polarizability of group-iiib elements,” *Phys. Rev. A* **91**, 052504 (2015).
- [57] S. Chattopadhyay, B. K. Mani, and D. Angom, “Electric dipole polarizability of alkaline-earth-metal atoms from perturbed relativistic coupled-cluster theory with triples,” *Phys. Rev. A* **89**, 022506 (2014).
- [58] R. Kumar, D. Angom, and B. K. Mani, “Fock-space perturbed relativistic coupled-cluster theory for electric dipole polarizability of one-valence atomic systems: Application to Al and In,” *Phys. Rev. A* **106**, 032801 (2022).